How to cite: *Angew. Chem. Int. Ed.* **2024**, *63*, e202414526
doi.org/10.1002/anie.202414526

Metal-Organic Frameworks

Regulated Charge Transfer in Donor-Acceptor Metal–Organic Frameworks for Highly-Sensitive Photodetectors

Zhiyun Xu, Abhinav Chandresh, Anna Mauri, Meysam Esmaeilpour, Vincent Monnier, Fabrice Odobel, Lars Heinke, Wolfgang Wenzel, Mariana Kozlowska, Stéphane Diring, Ritesh Haldar,* and Christof Wöll**

Abstract: In photo-induced charge separation, organic thin films with donor and acceptor chromophores are vital for uses such as artificial photosynthesis and photodetection. The main challenges include optimizing charge separation efficiency and identifying the ideal acceptor/donor ratio. Achieving this is difficult due to the variability in molecular configurations within these typically amorphous organic aggregates. Metal–organic frameworks (MOFs) provide a structured solution by enabling systematic design of donor/acceptor blends with adjustable ratios within a crystalline lattice. We demonstrate this approach by incorporating donor and acceptor naphthalenediimide (NDI) chromophores as linkers in a highly oriented, monolithic MOF thin film. By adjusting the NDI acceptor linker concentration during the layer-by-layer assembly of surface-anchored MOF thin films (SURMOFs), we significantly enhanced charge separation efficiency. Surprisingly, the optimum acceptor concentration was only 3 %, achieving a forty-fold increase in photodetection efficiency compared to baseline NDI donor-based SURMOFs. This unexpected behaviour was clarified through theoretical analysis enabled by the well-defined crystalline structure of the SURMOFs. Using density functional theory and kinetic Monte Carlo simulations, we identified two opposing effects from acceptors: the positive effect of suppressing undesirable charge carrier recombination is offset at high concentrations by a reduction in charge-carrier mobility.

Introduction

Mixtures of electron-rich (donor) and electron-deficient (acceptor) chromophores can undergo charge separation (CS) upon photoexcitation,[1] a process crucial for artificial photosynthesis,[2] diodes,[3] as well as for photodetectors.[4] Key factors influencing CS efficiency include the exciton binding energy of the light-absorbing chromophore (usually the donor),[5] the HOMO–LUMO gap of donor and acceptor,[5a,6] the relative positioning of the donor-acceptor pair,[7] and subsequent electron and hole mobility. While molecular design can control the first two factors,[8] predicting and regulating molecular packing—which is crucial for optimizing the relative positioning of donor-acceptor pairs and electron/hole mobility—remains challenging. This often necessitates trial-and-error approaches.[9] Additionally, the fabrication of organic thin films by drop-casting or spin-coating is highly sensitive to solvent medium and other physical parameters.[10]

A different approach to ensure well-defined relative positioning of donor-acceptor pairs involves the use of covalently bonded donor-acceptor chromophore constructs. These dyads have demonstrated charge separation and promising optoelectronic properties,[11] but achieving long-range order and coating larger surface areas with these compounds presents significant challenges.[12]

Furthermore, optimizing the donor-to-acceptor ratio is complicated by the difficulty in varying the structure of binary assemblies, as observed in previous studies.[13]

Crystalline metal–organic frameworks (MOFs) provide a powerful means to control the structure of organic donor-

[*] Dr. Z. Xu
College of Chemistry and Chemical Engineering
Central South University
410083 Changsha, China

Dr. Z. Xu, Dr. A. Chandresh, Prof. L. Heinke, Prof. C. Wöll
Institute of Functional Interfaces (IFG)
Karlsruhe Institute of Technology (KIT)
Hermann-von-Helmholtz-Platz 1
76344 Eggenstein-Leopoldshafen, Germany
E-mail: christof.woell@kit.edu

A. Mauri, Dr. M. Esmaeilpour, Prof. Dr. W. Wenzel, Dr. M. Kozlowska
Institute of Nanotechnology (INT)
Karlsruhe Institute of Technology (KIT)
Hermann-von-Helmholtz-Platz 1
76344 Eggenstein-Leopoldshafen, Germany

Dr. V. Monnier, Prof. F. Odobel, Dr. S. Diring
Nantes Université, CNRS
CEISAM, UMR 6230, F-44000 Nantes, France
E-mail: Stephane.Diring@univ-nantes.fr

Dr. R. Haldar
Tata Institute of Fundamental Research Hyderabad, Gopanpally,
Hyderabad 500046, Telangana, India
E-mail: riteshhaldar@tifrh.res.in

acceptor chromophore assemblies and achieve coherent crystalline order.[14] MOFs are formed by coordinating metal clusters with organic linkers,[15] i.e. organic donor and acceptor chromophores, with metal anchoring groups.[16] These materials offer several advantages over molecular solids formed by self-assembly: reduced degrees of freedom of the chromophores, facilitating decreased nonradiative decay processes;[17] periodic structures enabling exciton delocalization and charge carrier transport;[18] modifiability of individual chromophores without altering topology;[19] and predictable molecular packing.[20] Consequently, MOFs represent promising materials with numerous favorable optoelectronic properties.[21] The construction of framework with highly conjugated organic linkers, i.e., pentacene, perylene, and naphthalenediimide (NDI), can facilitate electron delocalization, resulting in enhanced charge transfer efficiency.[15b] Among them, core-substituted NDIs would be ideal for photoinduced charge transport owing to their unique attributes of rainbow fluorescence and tunable electronic properties.[1c] In this context, we made endeavors to optimize charge separation in oriented donor-acceptor framework based on NDI. Recent advancements in MOF thin film fabrication techniques,[22] such as chemical vapor deposition and layer-by-layer liquid-phase epitaxy,[23] address processability concerns and enable the exploration of optoelectronic functions on conducting substrates.[24]

In this context, we investigated the potential of creating a donor-acceptor MOF thin film capable of efficient free charge generation upon light exposure (Scheme 1). Due to the strong scattering effect in conventional MOF powders, accurate determination of photophysical properties is challenging. Therefore, we employ a layer-by-layer approach to grow homogeneous, monolithic MOF thin films (referred to as surface-mounted MOFs or SURMOFs) on functionalized substrates. We find that the optimal photocurrent response is achieved with a low concentration of acceptor linkers in a donor MOF, rather than a 1:1 donor/acceptor mixture. The resulting donor-acceptor MOF thin film exhibits a remarkably high photoresponse, with a photocurrent switching ratio of 1.1×10^4 and a detectivity of 1.48×10^{11} Jones—two orders of magnitude better than the pristine donor-MOF thin film. Through a combination of experimental and computational studies (including density functional theory and kinetic Monte Carlo simulation), we provide detailed insights into the exceptional photodetection ability of the novel donor-acceptor MOF thin film.

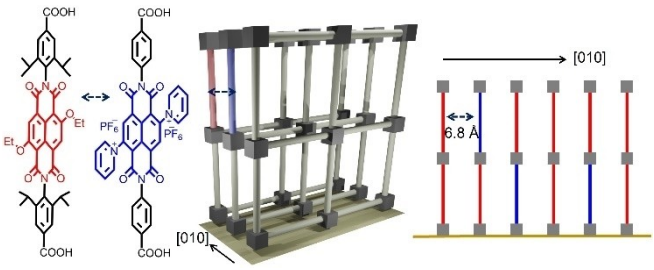

Scheme 1. An illustration of donor-acceptor MOF thin film grown in a layer-by-layer fashion to facilitate high photocurrent response. The donor (red) and acceptor (blue) linkers in the MOF structure are stacked in a 1D, along the [010] axis of the SURMOF-2 structure.

Results and Discussion

The current study is based on an important class of photoresponsive molecules, core-substituted naphthalenediimides (cNDIs).[25] Through the functionalization with -COOH anchoring groups, cNDIs can be converted to chromophoric MOF linkers, as demonstrated in earlier studies.[19] Here, two different core-substitutions were chosen; $NDIOEt_2$ and $NDIPy_2$ (for the synthesis procedure see the Supporting Information 1, Figure S1–S3), to realize an electron donor and an acceptor, respectively. To investigate whether these two cNDIs can form a donor-acceptor pair, we have calculated the highest occupied molecular orbital (HOMO) and the lowest unoccupied molecular orbital (LUMO) energy levels using density functional theory (DFT) and time-dependent DFT (see Supporting Information 1, Table S1). As shown in Figure 1a, the LUMO level of $NDIPy_2$ at −4.590 eV is substantially lower by approximately 1 eV than that of $NDIOEt_2$ at −3.650 eV. The chosen cNDIs thus fulfill a necessary requirement for a donor-acceptor pair. In previously reported SURMOF-2 assemblies of cNDIs the intermolecular distance between NDI linkers was estimated as 6.8 Å.[20] Calculations carried out for a donor-acceptor pair of $NDIOEt_2$ and $NDIPy_2$ with such a distance revealed that CS should be possible, as shown by the electron density difference in Figure 1b. Due to the good fit, the through-space charge transfer from the donor to the acceptor NDI chromophores should be straightforward.

MOFs of the type SURMOF-2 offer a straightforward way to assemble ditopic linkers into well-ordered arrays.[27] Since for Cu^{2+} units often unwanted quenching effects are

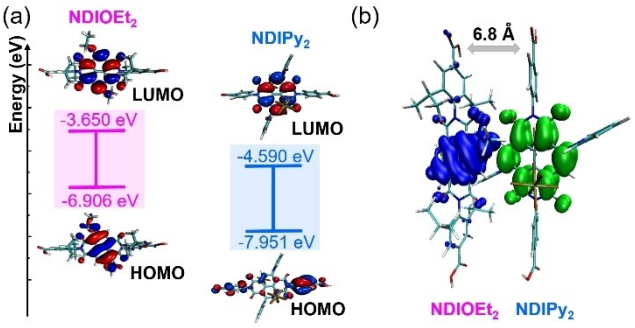

Figure 1. a) Visualization of HOMO and LUMO orbitals of $NDIOEt_2$ (left) and $NDIPy_2$ (right) with the corresponding frontier orbital energies. The energy of the LUMO orbital calculated as the sum of the HOMO energy and the first singlet-singlet excitation is −4.060 eV and −5.121 eV for $NDIOEt_2$ and $NDIPy_2$, respectively. b) Visualization of the electron density difference upon the singlet-singlet excitation (at 489 nm, see Table S2) of the dimer made out of $NDIOEt_2$ (left) and $NDIPy_2$ (right) on the modelled distance of 6.8 Å. The electron density depicting holes and electrons upon photoexcitation is marked in blue and green, respectively. All calculations were performed using B3LYP functional with def2-TZVP basis set and Grimme D3 (BJ) dispersion correction.[26] Further details are described in Supporting Information 1.

observed after irradiation with light, Zn was chosen as a metal node.[28] In a Zn-SURMOF-2 type structure, a similar arrangement of the donor-acceptor linkers is feasible (Scheme 1). The expected Zn-NDIOEt$_2$ SURMOF-2 type structure is shown in Figure 2a and Figure S4 (Supporting Information 1). In this MOF, linkers are stacked along [010] direction and the inter-linker distance was found to be ~6.8 Å.[20] According to the theoretical analysis (see above) such a packing is, in principle, well suited to allow for a photoinduced charge transfer if donor and acceptor linkers are mixed homogeneously. The corresponding scanning electron microscope (SEM) image shows the morphology and thickness of film (Figure 2b and Figure S5), while atomic force microscope (AFM) image offers the information of thickness and roughness (Figure S6). The thickness was measured to be ~300 nm, while the roughness was calculated to be ~10 nm. To synthesize such a donor-acceptor structure, we have fabricated SURMOF-2 films from NDIOEt$_2$/NDIPy$_2$ linker mixtures with relative acceptor concentrations of 1, 2, 3, 5, 20, and 50 %. As shown in Figure S7, Zn-NDIPy$_2$ has the same crystal lattice with Zn-NDIOEt$_2$. In all cases, well-defined and highly oriented thin films with the same crystalline structure were obtained, which is evidenced by the out-of-plane XRD patterns recorded for the mixed donor-acceptor SURMOFs (Figure 3a). All SURMOFs fabricated were characterized by infrared reflection absorption spectroscopy (Figure S8). To ensure that the acceptor-linker concentrations in the SURMOFs match those in the solutions used for the layer-by-layer process, energy dispersive X-ray spectroscopy was conducted (Figure S9, Supporting Information 1).

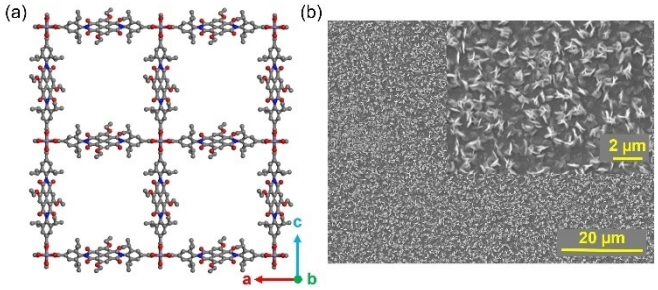

Figure 2. a) A simulated 2D layer structure of Zn-NDIOEt$_2$, b) SEM image of pristine Zn-NDIOEt$_2$.

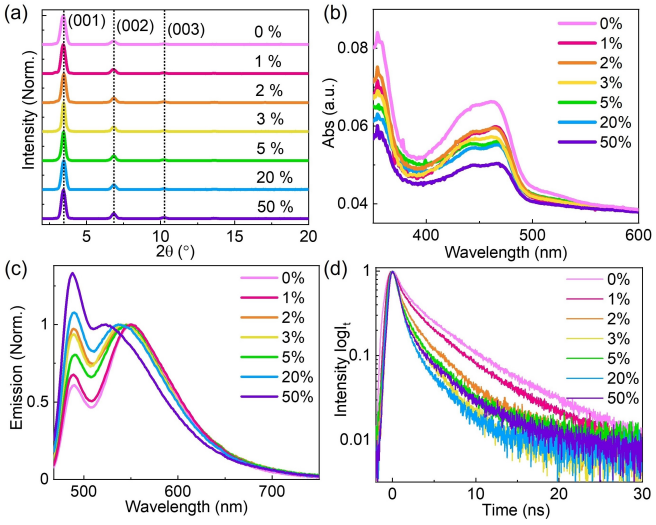

Figure 3. a) Out-of-plane XRD patterns of pristine Zn-NDIOEt$_2$ (with acceptor concentration of 0 %), as well as the mixed-linker SURMOFs with the acceptor concentrations of 1, 2, 3, 5, 20, and 50 %. b) Absorption spectra. c) Normalized photoluminescence spectra under the excitation of 450 nm. d) Logarithmic scale of fluorescence decay curves (excitation: 369 nm, emission: 550 nm).

To get an insight into the photophysical properties of the thin films, UV/Vis absorption and emission spectra were recorded (Figure 3b–d). The pristine Zn-NDIOEt$_2$ (**1**) displays strong absorption between 390 and 500 nm, related to J-type electronic coupling among the NDIOEt$_2$ linkers, as observed and assigned in an earlier report.[20] This J-aggregate yields bright green emission with a maximum at ~550 nm for **1**. Increasing the concentration of NDIPy$_2$ linkers in the mixed-linker thin films usually results in a decrease in emission intensity percentage and in lifetime reduction at ~550 nm (Figure 3d). At the same time, the intensity of the blue-shifted emission (~488 nm) originating from the NDIOEt$_2$ monomer was found to increase. This observation indicates that NDIPy$_2$ inhibits the J-coupling among the NDIOEt$_2$ linkers. At higher doping ratios, the J-aggregate emission peak (500–600 nm) exhibits a blue shift. This is attributed to an acceptor-induced rotation of the NDIOEt$_2$ linkers, which—at high doping ratios—alters the J-type electronic coupling among adjacent chromophores.

Note that while the changes in the emission spectra are rather obvious, the effect of doping on the absorption spectra is rather subtle, as Zn-NDIPy$_2$ (**2**) absorption (Figure S10, Supporting Information 1) is much weaker compared to Zn-NDIOEt$_2$. Further, the changes in emission profiles are very substantial at low doping levels, while further increases in the concentration of NDIPy$_2$ show fewer changes. This implies that doping is more homogeneous at lower concentrations of NDIPy$_2$. Overall, the photophysical studies confirm that the doping with the acceptor linker is successful, and distribution is more homogeneous for the lower % of NDIPy$_2$ in the mixed-linker thin films.

To realize efficient devices utilizing these mixed-linker thin films, SURMOFs were deposited on interdigitated gold electrodes, as shown in Figure 4a. The two-probe direct current (DC) between the two electrodes was measured under illumination with 455 nm light (power density 1.05 mW/cm^2) for a 1 V bias. As shown in Figure 4b, the dark current of pristine Zn-NDIOEt$_2$ is 0.008 nA, while the photocurrent reaches to 2.8 nA upon illumination, giving a switching ratio of 3.5×10^2. For the mixed-linker systems, a pronounced increase in these parameters is observed. The best performance was found for the film with 3 % acceptors, where the current changes dramatically from 0.011 nA to 121 nA upon illumination, corresponding to a switching ratio of 1.1×10^4. The photocurrent found in the film with 3 % acceptors is two orders of magnitude higher than that of the pristine film (**1**), indicating that proper mixing of the acceptor is an effective approach to improve photoresponse.

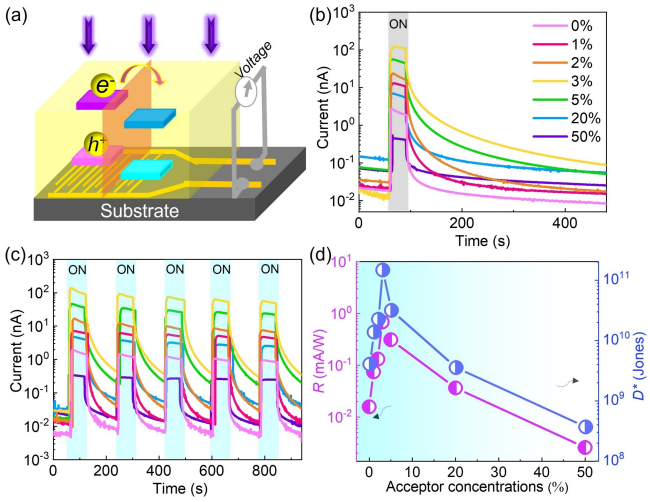

Figure 4. a). Planar devices based on SURMOFs under 1.05 mW/cm^2 of 455 nm with a bias voltage of 1 V. Photoinduced charge transfer occurs at the donor-acceptor interface (in orange). Electrons and holes are denoted as e^- and h^+, respectively. b). Photocurrent (I_{ph}) and dark current (I_{dark}). c) Time-dependent photocurrent under chopped light. d) Photoresponsivity R and detectivity D^* of mixed-linker SURMOFs. The effective area of the device amounts to 16.9 mm^2.

The highest photocurrent observed in the film with 3 % acceptors signifies the generation of the highest number of charge carriers, indicating that there is a more efficient separation of photoinduced electron-hole pairs.[29] Importantly, further increasing the concentration of the acceptor linker to 50 %, did not lead to a further increase in photoresponse, instead, a decrease was observed. (Figure 4b, Figure S11 (Supporting Information 1)). Such behavior is repeatable after several off-on cycles of visible light irradiation, as shown in Figure 4c.

The clear improvement of performance upon mixing with acceptors is also reflected by the photodetector's Figures of merit: photoresponsivity (R), and detectivity (D^*) (Figure 4d). Responsivity implies how efficiently the detector responds to light signals, while detectivity indicates the ability to detect extremely low irradiation power levels.[30] While for the pure donor film **1** we yield $R = 0.016$ mA/W and $D^* = 4.1\times10^9$ Jones (cmHz$^{1/2}$W^{-1}), for the film with 3 % acceptors we obtain $R = 0.68$ mA/W and $D^* = 1.48\times10^{11}$ Jones. This detectivity value is higher than 2D MOF $Fe_3(THT)_2(NH_4)_3$ ($D^* = 7\times10^8$ Jones)[31] and comparable with MOF thin film $Cu_3(C_{18}H_6(NH)_6)_2$ ($D^* = 3.2\times10^{11}$ Jones),[32] and even comparable with other photodetectors based on perovskites and inorganic complexes, including $CsPbCl_3$ ($D^* = 10^{10}$ Jones)[33] and CdTe($D^* = 1.02\times10^9$ Jones) (Supporting Information 1: Table S3).[34] The mixed-linker films containing a higher percentage of $NDIPy_2$ exhibit a poorer response than those with 3 % acceptors, as shown in Figure 4d. Moreover, the ambient humidity stabilities of high performance mixed-linker SURMOFs were confirmed by out-of-plane XRD patterns (Figure S12 and S13).[15c,d]

To better understand the reasons for this unexpectedly low optimum concentration of acceptors, kinetic Monte Carlo (KMC) simulations have been carried out for a 1D model system consisting of a 1D stack of 1000 linkers with varying ratios of donors and acceptors (see Supporting Information 2). In the donor-acceptor system considered, excitons are generated in the chromophoric MOF via $NDIOEt_2$ donors under light absorption and then dissociate to yield electrons and holes as a result of charge transfer at the donor-acceptor interface. These electrons and holes are then transported through the material as hole hopping via $NDIOEt_2$ and electron hopping to $NDIPy_2$. Finally, charge carriers are collected at gold electrodes resulting in a photocurrent. As shown in Figure 5, the current has a maximum which seems counterintuitive at first. As in calculation, we find that a significant number of hole charge carriers is generated for concentrations of acceptors around 3–7 %, with the maximal number of carriers found at a 5 % acceptor concentration. Increasing the concentration beyond this value leads to a rapidly diminishing current. At concentrations above 45 %, no charge carriers could be collected. To understand these results, we analyzed hole and electron current separately. In the absence of acceptors, photogenerated charge carriers recombine quickly and only a small photocurrent can be observed. Acceptors in the system act as electron traps, which suppress electron-hole recombination (see Figure 5 top). Since the probability of electron capture by acceptors increases with acceptor concentration, the current initially rises with acceptor concentration. Electrons cannot leave the acceptor, because the LUMO orbital of $NDIPy_2$ is much lower than the LUMO orbital of $NDIOEt_2$ (see Figure 1a). Moreover,

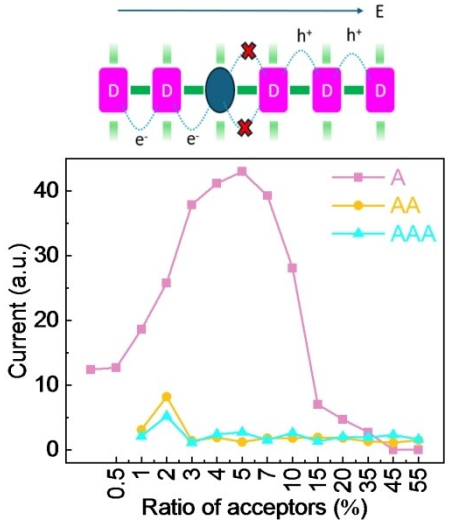

Figure 5. Bottom: Combined ambipolar current for a simulation of 1000 linker blocks obtained by the KMC simulation of charge transfer in a stack with donors (denoted in pink) and acceptors (marked with a ellipse). Top: Schematic visualization for allowed and disallowed hole (top) and electron (bottom) hopping process along the chain as a result of the applied electric field (denoted as E). Three types of morphologies were considered: acceptors homogeneously distributed between donors (A, in pink), acceptors distributed in pairs (AA, in yellow) and trimers (AAA, in blue). The plot represents the data obtained from ten independent KMC runs of 10^6 KMC steps each. The KMC protocol is described in the Supporting Information 2.

electron trapping processes may occur in the conditions considered,[35] additionally lowering the possibility of electron transport.

However, acceptors have a secondary effect in blocking the hole transport (Figure 5 top): We note that hole carriers cannot jump from the donor to the acceptor because the HOMO orbital of the acceptor is already occupied. Holes also do not hop from the acceptor to the donor, because the HOMO orbital of NDI-acceptors (ca. −7.951 eV, see Figure 1a) is lower than the HOMO orbital of $NDIOEt_2$ donors (ca. −6.906 eV). Considering the motion of a hole in the direction of the electric field, holes can move along the chain until they are blocked by an acceptor site, which they can circumvent only using a diffusive mechanism. As a result, an increasing acceptor concentration reduces the average velocity with which the holes can travel, counterbalancing the effect of suppressed recombination. The interplay of these effects results in the observed maximum of the current.

While the total concentration of acceptors is known, it is difficult to determine experimentally whether acceptor clustering has a significant effect. As shown in Figure 5, we find that acceptor clustering would lead to almost vanishing currents and a maximum of the current at even smaller concentrations. The KMC simulation result displayed by the pink curve (A) in Figure 5 agrees well with the experimental findings and demonstrates that acceptor-based linkers should be homogeneously distributed in the MOF sample. Both the theoretical and experimental results confirm that low doping concentrations, as well as CS on donors realized by neighboring electron acceptors, greatly favor charge transport.

Conclusion

In conclusion, we have demonstrated that using the metal–organic framework approach enables to organize electron donors and acceptors in an optimized configuration and distribution to realize efficient charge separation. Using the layer-by-layer method, donor-acceptor MOF thin films were fabricated. Photocurrent measurements of those thin films in device configuration disclosed that at a low optimal doping concentration (3 %), charge carrier generation is the highest. The superior performance is evident from a high photocurrent switching ratio of 1.1×10^4, and a detectivity of 1.48×10^{11} Jones. Such high performance can be attributed to efficient donor-acceptor interaction between NDI-donor and NDI-acceptor followed by distance-separated charge transfer, hampering charge recombination. Hole transport within NDI-donors, modulating the photocurrent measured, is significantly improved, when the concentration of NDI-acceptors is low. The latter originates from the homogeneous distribution of donors and acceptors in the SURMOF, efficient distance-separated charge transfer, lowering charge recombination, and the favorable difference in LUMO level between $NDIOEt_2$ and $NDIPy_2$. The findings pave the way towards improvement of optoelectronic performance of MOF films by tuning charge transfer interaction through adjusting donor-acceptor ratios in oriented donor-acceptor framework and offer new strategy for development of high-performance optoelectronic devices.

Supporting Information

The authors have cited additional references within the Supporting Information.[36–51] The results of the KMC simulations and DFT calculations are available via the NOMAD repository under https://doi.org/10.17172/NOMAD/2024.07.29-1.

Acknowledgements

Z.X. acknowledges the financial support from Scientific Research Foundation by Central South University (no. 502044027). S.D. acknowledges the financial support from the ANR PhotoMOF project, Grant ANR-18-CE05-0008-01. This research has been funded by Deutsche Forschungsgemeinschaft (DFG, German Research Foundation) under Germany's Excellence Strategy for the Excellence Cluster "3D Matter Made to Order" (Grant No. EXC-2082/1-390761711) and by the Carl Zeiss Foundation. M.E., W.W. and M.K. acknowledge funding within GRK 2450 "Scale bridging methods of computational nanoscience" and the Virtual Materials Design initiative (VirtMat) at KIT. The authors acknowledge support by the state of Baden-Württemberg through bwHPC and the German Research Foundation (DFG) through grant no INST 40/575-1 FUGG (JUSTUS 2 cluster) under project bw20F004. RH acknowledges Council of Scientific and Industrial Research (CSIR), Govt of India, extramural grant no. 01/3116/23/EMR-II and intramural funds at TIFR Hyderabad from the Department of Atomic Energy (DAE), India, under Project Identification Number RTI 4007. Open Access funding enabled and organized by Projekt DEAL.

Conflict of Interest

The authors declare no conflict of interest.

Data Availability Statement

The data that support the findings of this study are available in the supplementary material of this article.

Keywords: naphthalenediimide · charge transfer · donor-acceptor · metal–organic framework thin films · photodetectors

[1] a) H. Tamura, I. Burghardt, *J. Am. Chem. Soc.* **2013**, *135*, 16364–16367; b) D. A. Vithanage, A. Devizis, V. Abramavicius, Y. Infahsaeng, D. Abramavicius, R. C. I. MacKenzie, P. E. Keivanidis, A. Yartsev, D. Hertel, J. Nelson, V. Sundstrom, V.

Gulbinas, *Nat. Commun.* **2013**, *4*, 2334; c) S. V. Bhosale, C. H. Jani, S. J. Langford, *Chem. Soc. Rev.* **2008**, *37*, 331–342.
[2] a) T. M. Clarke, J. R. Durrant, *Chem. Rev.* **2010**, *110*, 6736–6767; b) M. R. Wasielewski, *Chem. Rev.* **1992**, *92*, 435–461.
[3] a) S. Gélinas, A. Rao, A. Kumar, S. L. Smith, A. W. Chin, J. Clark, T. S. van der Poll, G. C. Bazan, R. H. Friend, *Science* **2014**, *343*, 512–516; b) G. Yu, A. J. Heeger, *J. Appl. Phys.* **1995**, *78*, 4510–4515.
[4] H. Ren, J. D. Chen, Y. Q. Li, J. X. Tang, *Adv. Sci.* **2021**, *8*, 2002418.
[5] a) G. J. Hedley, A. Ruseckas, I. D. W. Samuel, *Chem. Rev.* **2017**, *117*, 796–837; b) I. G. Hill, A. Kahn, Z. G. Soos, R. A. Pascal, *Chem. Phys. Lett.* **2000**, *327*, 181–188; c) M. Knupfer, *Appl. Phys. A* **2003**, *77*, 623–626.
[6] D. Z. Yang, D. G. Ma, *Adv. Opt. Mater.* **2019**, *7*, 1800522.
[7] a) Y. Q. Hou, X. Zhang, K. P. Chen, D. Y. Liu, Z. J. Wang, Q. Y. Liu, J. Z. Zhao, A. Barbon, *J. Mater. Chem. C* **2019**, *7*, 12048–12074; b) O. V. Mikhnenko, P. W. M. Blom, T. Q. Nguyen, *Energy Environ. Sci.* **2015**, *8*, 1867–1888; c) B. Carsten, J. M. Szarko, H. J. Son, W. Wang, L. Y. Lu, F. He, B. S. Rolczynski, S. J. Lou, L. X. Chen, L. P. Yu, *J. Am. Chem. Soc.* **2011**, *133*, 20468–20475.
[8] H. Imahori, T. Umeyama, K. Kurotobi, Y. Takano, *Chem. Commun.* **2012**, *48*, 4032–4045.
[9] a) C. F. Leong, B. Chan, T. B. Faust, D. M. D'Alessandro, *Chem. Sci.* **2014**, *5*, 4724–4728; b) M. Polkehn, H. Tamura, P. Eisenbrandt, S. Haacke, S. Mery, I. Burghardt, *J. Phys. Chem. Lett.* **2016**, *7*, 1327–1334; c) M. Frank, J. Ahrens, I. Bejenke, M. Krick, D. Schwarzer, G. H. Clever, *J. Am. Chem. Soc.* **2016**, *138*, 8279–8287; d) H. Kang, W. Lee, J. Oh, T. Kim, C. Lee, B. J. Kim, *Acc. Chem. Res.* **2016**, *49*, 2424–2434.
[10] K. S. Mali, M. G. Schwab, X. L. Feng, K. Müllen, S. De Feyter, *Phys. Chem. Chem. Phys.* **2013**, *15*, 12495–12503.
[11] a) H. Q. Li, P. P. Shao, S. Q. Chen, G. S. Li, X. Feng, X. Chen, H. J. Zhang, J. B. Lin, Y. B. Jiang, *J. Am. Chem. Soc.* **2020**, *142*, 3712–3717; b) N. Keller, T. Bein, *Chem. Soc. Rev.* **2021**, *50*, 1813–1845; c) S. Jin, X. Ding, X. Feng, M. Supur, K. Furukawa, S. Takahashi, M. Addicoat, M. E. El-Khouly, T. Nakamura, S. Irle, S. Fukuzumi, A. Nagai, D. Jiang, *Angew. Chem. Int. Ed.* **2013**, *52*, 2017–2021.
[12] a) J. W. Zhao, J. Y. Ren, G. Zhang, Z. Q. Zhao, S. Y. Liu, W. D. Zhang, L. Chen, *Chem. Eur. J.* **2021**, *27*, 10781–10797; b) M. Madhu, R. Ramakrishnan, V. Vijay, M. Hariharan, *Chem. Rev.* **2021**, *121*, 8234–8284; c) X. Li, X. Yue, Y. Wang, T. Chen, Y. Zhou, D. Liu, H. Xiang, S. Zhang, H. Zeng, Z. Xiang, *eScience* **2023**, *3*, 100084.
[13] a) S. W. Ko, R. Mondal, C. Risko, J. K. Lee, S. H. Hong, M. D. McGehee, J. L. Brédas, Z. A. Bao, *Macromolecules* **2010**, *43*, 6685–6698; b) Q. Peng, K. Park, T. Lin, M. Durstock, L. Dai, *J. Phys. Chem. B* **2008**, *112*, 2801–2808.
[14] a) R. Haldar, L. Heinke, C. Wöll, *Adv. Mater.* **2020**, *32*, 1905227; b) N. Sikdar, A. Hazra, D. Samanta, R. Haldar, T. K. Maji, *Angew. Chem. Int. Ed.* **2020**, *59*, 18479–18484.
[15] a) N. Stock, S. Biswas, *Chem. Rev.* **2012**, *112*, 933–969; b) J. J. Liu, Y. Zhou, Z. Xie, Y. Li, Y. P. Liu, J. Sun, Y. H. Ma, O. S. M. Terasaki, L. Chen, *Angew. Chem. Int. Ed.* **2020**, *59*, 1081–1086; c) M. J. Velasquez-Hernandez, M. Linares-Moreau, L. A. Brandner, B. Marmiroli, M. Barella, G. P. Acuna, S. D. Zilio, M. F. K. Verstreken, D. E. Kravchenko, O. M. Linder-Patton, J. D. Evans, H. Wiltsche, F. Carraro, H. Wolinski, R. Ameloot, C. Doonan, P. Falcaro, *Adv. Mater.* **2023**, *35*, e2211478; d) L. A. Brandner, M. Linares-Moreau, G. Zhou, H. Amenitsch, S. Dal Zilio, Z. Huang, C. Doonan, P. Falcaro, *Chem. Sci.* **2023**, *14*, 12056–12067.
[16] R. Haldar, H. Y. Chen, A. Mazel, D. H. Chen, G. Gupta, N. Dua, S. Diring, F. Odobel, C. Wöll, *Adv. Mater. Interfaces* **2021**, *8*, 2100262.
[17] N. B. Shustova, B. D. McCarthy, M. Dinca, *J. Am. Chem. Soc.* **2011**, *133*, 20126–20129.
[18] R. Haldar, M. Jakoby, A. Mazel, Q. Zhang, A. Welle, T. Mohamed, P. Krolla, W. Wenzel, S. Diring, F. Odobel, B. S. Richards, I. A. Howard, C. Wöll, *Nat. Commun.* **2018**, *9*, 4332.
[19] R. Haldar, A. Mazel, R. Joseph, M. Adams, I. A. Howard, B. S. Richards, M. Tsotsalas, E. Redel, S. Diring, F. Odobel, C. Wöll, *Chem. Eur. J.* **2017**, *23*, 14316–14322.
[20] R. Haldar, A. Mazel, M. Krstic, Q. Zhang, M. Jakoby, I. A. Howard, B. S. Richards, N. Jung, D. Jacquemin, S. Diring, W. Wenzel, F. Odobel, C. Wöll, *Nat. Commun.* **2019**, *10*, 2048.
[21] a) X. J. Liu, M. Kozlowska, T. Okkali, D. Wagner, T. Higashino, G. Brenner-Weifss, S. M. Marschner, Z. H. Fu, Q. Zhang, H. Imahori, S. Brase, W. Wenzel, C. Wöll, L. Heinke, *Angew. Chem. Int. Ed.* **2019**, *58*, 9590–9595; b) B. Zhang, B. B. Qian, C. T. Li, X. W. Li, H. X. Nie, M. H. Yu, Z. Chang, *CrystEngComm* **2022**, *24*, 5538–5551.
[22] a) C. Crivello, S. Sevim, O. Graniel, C. Franco, S. Pané, J. Puigmartí-Luis, D. Muñoz-Rojas, *Mater. Horiz.* **2021**, *8*, 168–178; b) O. Shekhah, J. Liu, R. A. Fischer, C. Wöll, *Chem. Soc. Rev.* **2011**, *40*, 1081–1106; c) Z. Fu, G. Xu, *Chem. Rec.* **2017**, *17*, 518–534; d) A. Betard, R. A. Fischer, *Chem. Rev.* **2012**, *112*, 1055–1083.
[23] a) J. Liu, C. Wöll, *Chem. Soc. Rev.* **2017**, *46*, 5730–5770; b) I. Stassen, M. Styles, G. Grenci, H. V. Gorp, W. Vanderlinden, S. D. Feyter, P. Falcaro, D. D. Vos, P. Vereecken, R. Ameloot, *Nat. Mater.* **2016**, *15*, 304–310; c) M. Choe, J. Y. Koo, I. Park, H. Ohtsu, J. H. Shim, H. C. Choi, S. S. Park, *J. Am. Chem. Soc.* **2022**, *144*, 16726–16731; d) L. Heinke, C. Wöll, *Adv. Mater.* **2019**, *31*, e1806324.
[24] a) V. Stavila, A. A. Talin, M. D. Allendorf, *Chem. Soc. Rev.* **2014**, *43*, 5994–6010; b) R. Haldar, L. Heinke, C. Wöll, *Adv. Mater.* **2020**, *32*, e1905227.
[25] N. Sakai, J. Mareda, E. Vauthey, S. Matile, *Chem. Commun.* **2010**, *46*, 4225–4237.
[26] a) S. Grimme, S. Ehrlich, L. Goerigk, *J. Comput. Chem.* **2011**, *32*, 1456–1465; b) K. Raghavachari, *Theor. Chem. Acc.* **2000**, *103*, 361–363; c) A. Schafer, H. Horn, R. Ahlrichs, *J. Chem. Phys.* **1992**, *97*, 2571–2577.
[27] J. Liu, B. Lukose, O. Shekhah, H. K. Arslan, P. Weidler, H. Gliemann, S. Brase, S. Grosjean, A. Godt, X. Feng, K. Müllen, I. B. Magdau, T. Heine, C. Wöll, *Sci. Rep.* **2012**, *2*, 921.
[28] M. D. Allendorf, C. A. Bauer, R. K. Bhakta, R. J. T. Houk, *Chem. Soc. Rev.* **2009**, *38*, 1330–1352.
[29] H. Liu, C. Y. Xu, D. D. Li, H. L. Jiang, *Angew. Chem. Int. Ed.* **2018**, *57*, 5379–5383.
[30] Z. Xu, Y. Li, X. Liu, C. Ji, H. Chen, L. Li, S. Han, M. Hong, J. Luo, Z. Sun, *Adv. Opt. Mater.* **2019**, *7*, 1900308.
[31] H. Arora, R. H. Dong, T. Venanzi, J. Zscharschuch, H. Schneider, M. Helm, X. L. Feng, E. Cánovas, A. Erbe, *Adv. Mater.* **2020**, *32*, 1907063.
[32] L. A. Cao, M. S. Yao, H. J. Jiang, S. Kitagawa, X. L. Ye, W. H. Li, G. Xu, *J. Mater. Chem. A* **2020**, *8*, 9085–9090.
[33] Z. Y. Rao, W. Y. Liang, H. M. Huang, J. Ge, W. L. Wang, S. S. Pan, *Opt. Mater. Express* **2020**, *10*, 1374–1382.
[34] R. Q. Cheng, Y. Wen, L. Yin, F. M. Wang, F. Wang, K. L. Liu, T. A. Shifa, J. Li, C. Jiang, Z. X. Wang, J. He, *Adv. Mater.* **2017**, *29*, 1703122.
[35] A. Saeki, S. Seki, S. Tagawa, *J. Appl. Phys.* **2006**, *100*, 023703.
[36] SimStack. The Boost for Computer Aided-Design of Advanced Materials, https://www.simstack.de/, **2023**.
[37] A. D. Becke, *J. Chem. Phys.* **1993**, *98*, 5648–5652.
[38] G. Scalmani, M. J. Frisch, *J. Chem. Phys.* **2010**, *132*, 114110.
[39] M. J. Frisch, G. W. Trucks, H. B. Schlegel, G. E. Scuseria, M. A. Robb, J. R. Cheeseman, G. Scalmani, V. P. Barone, G. A. Petersson, H. Nakatsuji, X. Li, Gaussian 16, Gaussian, Inc., Wallingford CT, **2016**.

[40] T. Lu, F. W. Chen, *J. Comput. Chem.* **2012**, *33*, 580–592.
[41] M. H. Tran, J. Hur, *Adv. Opt. Mater.* **2022**, *10*, 2101404.
[42] T. M. H. Nguyen, C. W. Bark, *ACS Appl. Mater. Interfaces* **2023**, *14*, 45573–45581.
[43] Y. B. Tian, N. Vankova, P. Weidler, A. Kuc, T. Heine, C. Wöll, Z. G. Gu, J. Zhang, *Adv. Sci.* **2021**, *8*, 2100548.
[44] Z. T. Du, D. F. Fu, T. Yang, Z. Fang, W. N. Liu, F. M. Gao, L. Wang, Z. B. Yang, J. Teng, H. Zhang, W. Y. Yang, *J. Mater. Chem. C* **2018**, *6*, 6287–6296.
[45] Y. T. Chen, Y. L. Chu, X. H. Wu, O. Y. Wei, H. Jia, *Adv. Mater.* **2017**, *29*, 1704062.
[46] V. Adinolfi, O. Ouellette, M. I. Saidaminov, G. Walters, A. L. Abdelhady, O. M. Bakr, E. H. Sargent, *Adv. Mater.* **2016**, *28*, 7264–7268.
[47] Y. Wang, R. Fullon, M. Acerce, C. E. Petoukhoff, J. Yang, C. G. Chen, S. N. Du, S. K. Lai, S. P. Lau, D. Voiry, D. O'Carroll, G. Gupta, A. D. Mohite, S. D. Zhang, H. Zhou, M. Chhowalla, *Adv. Mater.* **2017**, *29*, 1603995.
[48] L. Wang, J. Jie, Z. Shao, Q. Zhang, X. Zhang, Y. Wang, Z. Sun, S.-T. Lee, *Adv. Funct. Mater.* **2015**, *25*, 2910–2919.
[49] L. Li, W. K. Wang, Y. Chai, H. Q. Li, M. L. Tian, T. Y. Zhai, *Adv. Funct. Mater.* **2017**, *27*, 1701011.
[50] J. Zhou, M. Xie, H. Ji, A. Cui, Y. Ye, K. Jiang, L. Shang, J. Zhang, Z. Hu, J. Chu, *ACS Appl. Mater. Interfaces* **2020**, *12*, 18674–18682.
[51] J. Li, X. Xi, S. Lin, Z. H. Ma, X. D. Li, L. X. Zhao, *ACS Appl. Mater. Interfaces* **2020**, *12*, 11965–11971.

Manuscript received: July 31, 2024
Accepted manuscript online: November 12, 2024
Version of record online: November 26, 2024